Improving the system performance of DWDM-FSO through combination of adaptive detection threshold and modified OOK under atmospheric turbulence, crosstalk, and ASE noise

Mohammed Raisan Hayal [*1] (ID)**, Ebrahim Eldesoky Elsayed** [2] (ID)

[1] *Electronics and Communications Engineering Department, Faculty of Engineering, Mansoura University, Mansoura 35516, El-Dakahlia Governorate, Egypt*
[2] *Electronics and Communications Engineering Department, Faculty of Engineering, Mansoura University, Mansoura 35516, El-Dakahlia Governorate, Egypt*

Abstract
The article delves into the intricate design and analysis of the dense wavelength division multiplexing free-space optical (DWDM-FSO) communication systems, focusing on the impact of modified on-off keying (OOK) modulation on various factors such as noise, interchannel crosstalk, and atmospheric turbulence in different turbulence conditions. Through in-depth numerical studies, it has been observed that the utilization of adaptive detection threshold alongside OOK modulation can lead to the occurrence of an error floor within the DWDM-FSO link. This suggests that careful consideration and optimization of these modulation techniques are paramount in ensuring the efficiency and reliability of communication systems operating under varying atmospheric conditions. This study sheds light on the complexities and challenges involved in DWDM-FSO systems and underscores the importance of tailored modulation strategies to mitigate potential issues and enhance overall performance.

1. Introduction

While concerning communication signals within the system of dense wavelength division multiplexing (DWDM) associated to free-space optical (FSO) system transversing through requirements in the radio individually ignoring with the permissions licensed through spectrum analysis given with security, and transmitting data which can be hampered by the regular fluctuations in the pressure and temperature that happen over atmosphere conditions [1], [2]. When such systems adjust irradiance and identify immediately using

persistent thresholds besides error floors, and on-off keying that initiates under formulation towards the ratio of extreme signal-to-noise ratios (SNRs) under the analysis [3], [4]. Further, the claims given moderately drawn in the thresholds adjustments combined to on-off keying (OOK), that ignores each of them [5]. For the change in the power received (signal + crosstalk), there is in absence of noise which can threshold for the decision associate for regular mode into the limits sets to responsivity × (signal average power + crosstalk average power) that enables the nominal data subjects with the turbulence of signal case into the attributes. Moreover, the wavelength given under the data of recovered preference given under crosswalk for nominal region into the increment range of nominal power. Regardless of the signal or the turbulence cause of crosswalk, the data can be carried to the time fractional to the power impacted to the states of being fed in the network [1]-[6]. When scintillation states fall within this percentage attributed to the framework crosstalk "guesstimates" subjected for the half of the signal durational to the uncorrelated form of data attained for signal and crosstalk, given for the obtained error probability occurred in the unit of bit-error-rate, referred to "BER," at 0.5 quantity. In the more common scenario where the nominal signal that can power overdoes the nominal power associates with crosstalk (without regard for scenario, i.e., the crosstalk turbulence or within the signal aforementioned can be impacted), occurring towards the data acquired to the wavelength ahead recovered in the data attributed to crosstalk. To create the greater quantity within the BER under unique states of scintillation makes the estimate to zero. Consequently, the error floor is obtained for nominal range of BER at the estimate given as: $0.5 × F + 0 × (1-F) = F/2$, where F in the formulation defines the time is fractional with certainly provided attributes such as ASE, internchannel crosstalk, noise, and atmospheric turbulence (AT) are superior to signal, moreover the nominal can be propagated to each state under scintillation reached within the probability density function (pdf) occurring through Rytov variance individually [6]. To make it easier, the departures are visualized based on the error floor under lower range of powered signals that can be injected into the noise quantity injected to the minimal quantity of the system. Nevertheless, for appropriate extreme powered signal, this insignificant noise which eliminates further to level of error insisted for such scenario. Under reasoning through the connections implied in BER for dependable to nominal product of power being generated for the system. In particular, the definition of F implies BER is independent to nominal signal received to the power, even when BER = F/2. Furthermore, the graphs cannot be duplicated using the floors they display. In particular, Figure 2a in [6] shows the initial error floor. This figure shows, among other things, how BER varies with nominal power received in optical region for following scenarios: There exists three possible scenarios: signal turbulence but no interferer (TurbuSi); no interferer or turbulence (Si); and an interferer but only turbulence in the signal (TurbuSi, XT). Besides, the arrangement of this document is as develops. The DWDM-FSO system design with eight channels and two transmitter and receiver sections was provided in Section 2. In Section 3, the error floor in the case of an adaptive threshold is examined numerically. In Section 4, we clarify the subtleties involved in computing an adaptive detection threshold. The revised OOK modulation is provided in Section 5. The eye diagram and quality factor simulation results for the DWDM–FSO with return-to-zero (RZ) and non-return-to-zero (NRZ) are shown in the last section.

2. System Design

By expanding the number of channels, DWDM-FSO links can improve technical capacity and facilitate long-distance data transfer. Wavelength division multiplexing, or WDM, comes in three regularly utilized varieties: broadband WDM, dense WDM, and coarse WDM. Most commonly identified C-band associates with the wavelength ranged from 1540 nm to 1569 nm. Within the multiplexes that carry with the band of multiple optical range signals in which the technology of DWDM associated under distinct channel through separate indications by substantial frequency dimensions. It also helps to reduce usage of bandwidth which facilitates the reach in the capacity attainment for Terabits per second, making it easier to the data rate increment within linkage of FSO scheme [6] [7]. Based on technologies of network accessible within the structure of copper material that can replace eventually under the passive optical networks (PON) analysis, which serve as the preceding range linking concerning distinct residences besides businesses in addition to foremost system [8], [9]. Furthermore, the subsequent initiation for the distribution under the network accessible with FSO, referred to as WDM, provides greater bandwidth [10], [11–14]. In order to fully utilize the large assigning bandwidth offered in the domain of optical field, (WDM-PON) sets established wavelengths under every optical network unit (ONU) associated to the program [12], [13]. Comparing (WDM-PON) systems to time-division-multiple access (TDM/TDMA) classifications, the earlier offer reduced loss, more bandwidth, and increased security [6, 7, 14–20].
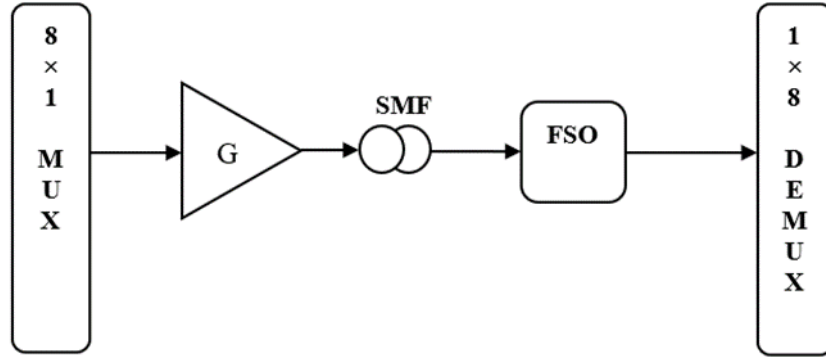
Figure 1. Illustration of DWDM with linkage of FSO.

2.1. Transmitter Module

To attain stability, we have employed an externally modulated transmitter in the transmitter part. Additionally, this lessens non-linear effects and chirps [6, 15]. Here, digital data is generated using the pseudo random bit sequence (PRBS), and digital signals are converted into electrical signals using an NRZ pulse generator. Subsequently, the modulator combines the electrical signal with the input signal from the light source to produce an optical signal outcome subsequently fed through multiplexer channel. Eight transmitters with a frequency arrangement of 100 GHz each, starting at 1550 nm and a feeder fiber length of 20 km, are employed in our system [6], [18–20].

2.2. Receiver Module

To detect signals in optical motions, translate the signals into electrical nature, in addition transmit its converted signals into low-pass Bessel filtering process that allows low range frequencies, rejecting the high range frequencies, further sectional to the receiver outcome linked to the PIN configured to photo-detector [2], [6].

Figure 2. Receiver scheme.

3. Adaptive Threshold Numerically: The Error Floor

In Equations (1) and (2), we can see the relationship between BER for both signal, interference and thermal noise variance. The notations that are generally used are used in the following, and unless otherwise stated, all values are presented in SI units. The reliance in the first scenario is as follows [2], [6], [18–21]:

$$BER\left(P_{R,sig}(1)\right) = \frac{1}{4}\,\mathrm{erfc}\left(\frac{2(r-1)RP_{R,sig}(1)/(r+1)}{2qB_e RP_{R,sig}(1)+\sigma_{th}^2}\right) \tag{1}$$

In the subsequent instance, it possesses a framework

$$BER = \frac{1}{4}\int_0^\infty \mathrm{erfc}\left(\frac{2(r-1)R\cdot P/(r+1)}{2qB_e R\cdot P+\sigma_{th}^2}\right)p_{GG}\left(\frac{P}{P_{R,sig}(1)}\right)dP \tag{2}$$

where

$$p_{GG}\left(\frac{P}{P_{R,sig}(1)}\right) = \frac{2(\alpha\beta)^{(\alpha+\beta)/2}}{\Gamma(\alpha)\Gamma(\beta)}\left(\frac{P}{P_{R,sig}(1)}\right)^{\frac{\alpha+\beta}{2}-1} \times K_{\alpha-\beta}\left(2\sqrt{\alpha\beta\frac{P}{P_{R,sig}(1)}}\right). \tag{3}$$

Lastly, the reliance in the final scenario is as follows [6], [18–21]:

$$BER = \frac{1}{4} \int_0^\infty \mathrm{erfc}\left(\frac{2(r-1)R \cdot P(1 - 1/C_{XT})/(r+1)}{2qB_e R \cdot P(1 + 1/C_{XT}) + \sigma_{th}^2} \right) \times P_{GG}\left(\frac{P}{P_{R,sig}(1)} \right) dP.$$ (4)

where the large and tiny scattering, respectively, are represented by the values α and β in [6]. In fact, it is challenging for verifying the precise input attributes which are utilized in the study [6] because of how ambiguously it is stated. We think that the subsequent input attribute estimates conferred in SI units measurements are sufficient to duplicate the graphical analysis illustrated under figure 2a in [6] below evaluation which is consistent with aforementioned arguments: C_{XT} ratio under signal-to-crosstalk, $R_b = 2.5 \cdot 10^9$ gives the data rate, $m_t = 2$ is the ASE quantity of polarization states, the extinction ratio $r = 10$, $\eta = 1$ is quantum efficiency, $\lambda = 1.55 \cdot 10^6$, $B_0 = 60 \cdot 10^9$ gives the optical channel bandwidth, the electrical bandwidth $B_e = R_b/2$, $N_0 = 0$ signifies the single-polarization based ASE power attributed with the spectral-density noise, total thermal noise variance $\sigma_{th}^2 = 98 \cdot 10^{-14}$, $l_{fso} = 1000$, associated under collective lens to receiving diameter $D_{RX} = 0.017$. Our computer findings are shown in Figure 3. As can be observed, case #3 does not have an error floor. As such, it makes sense to check that the computations are adequate. For computation of the integrals over time within the accurate right-hand side (RHS) of the equation, the primary difficulty is on Equations (3) and (4) at the identified attribute of Gamma-Gamma (GG) pdf p_GG.
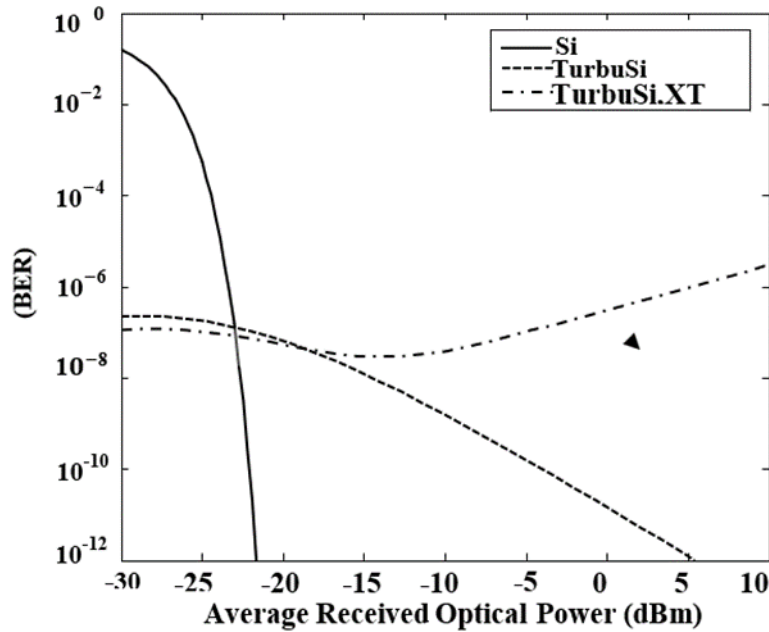

Figure 3. BER for turbulence regimes with respect to the average received optical power(dBm) C_n^2 = 1e-13m$^{-\frac{2}{3}}$ dna, C_{XT}= 30dB

4. Adaptive Threshold Numerically: The Error Floor

We introduce the computation for an adaptive detection threshold from Eqs. (5) and (6). For the accurate value determination over the limits of integration within the formulations. Thus, the dependencies followed are stated in [6], [15], [16], [18–25], should be examined:

$$p_{GG}(h_X) = \frac{2(\alpha\beta)^{(\alpha+\beta)/2}}{\Gamma(\alpha)\Gamma(\beta)} (h_X)^{\frac{\alpha+\beta}{2}-1} K_{\alpha-\beta}\left(2\sqrt{\alpha\beta h_X}\right)$$ (5)

where h_X is the attenuation due to AT [6], 18-20]

Since

$$\int_{10^{-12}}^{3} p_{GG}(h_X) dh_X = 0.9725,$$ (6)

Integrations are carried out in formulations of Eqs. (2) to (7) within the range of $10^{-12} \cdot P_{R,sig}(1)$ to $3 \cdot P_{R,sig}(1)$ you may rely on an accuracy of no more than a few percent. Figure 3 displays the GG pdf's dependency on h_X.

With the graph of h_X replaces over 10^{-12} to 3. It can be inferred from Figure 3 illustrates no certain locations within the gradients dealt for the intervals sequenced. Consequently, while executing combinations, a uniform grid can be used. To achieve the outcomes shown in below, there should be propagation through which spectrum acquired to the range of P as of $10^{-12} \cdot P_{R,sig}(1)$ till $3 \cdot P_{R,sig}(1)$ under consistent framework, which has about 72011 connections. We compute the % estimate of maximum amount of deviation occurred and vice versa under identical computations within the uniformity followed for the framework with 36011 connections to determine if it is sufficient. The variances in Cases 2 and 3 are also significantly less than 1%. The selected grid is thus sufficiently dense. Surprisingly, by a numerical experiment, we were able to determine the BER dependencies over the nominal count of optical power received in the case of 3 scenarios indicated overhead, which correspond considerably more closely as that shown in [6] instead with the performance achieved in illustration of Figure 3 (refer to Figure 5).
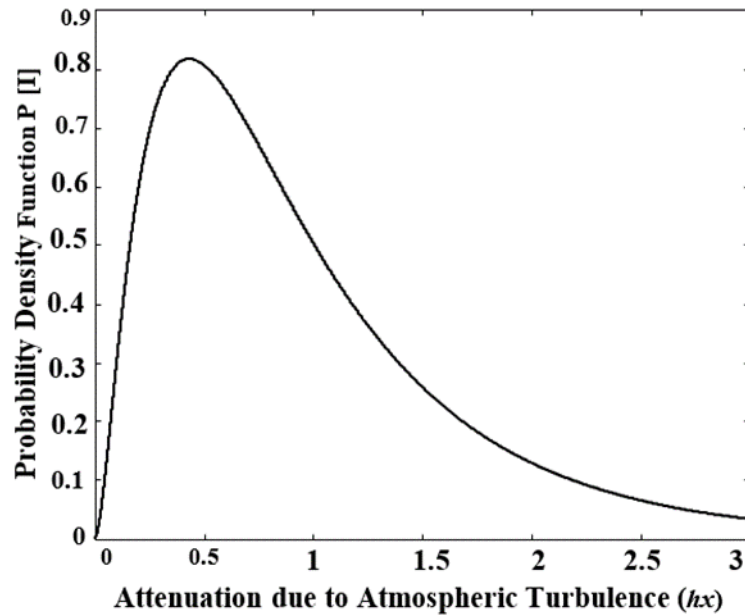

Figure 4. Attenuation for PDF owing to AT (h_x).

5. Modified Ook

These are the details that describe the experiment. Using the uniform grid with 20001 points, one can select a value that is nearly zero for the integrals' goes with lower limit and a quantity that is significantly larger than the first number for the upper limit. For example, one can aim for both the upper and lower limit. Nonetheless, the GG pdf may normalize to a value that is not quite equal to 1 as a result of the arbitrary limit selection. Consequently, the A constant attributed to the normalization factor within the function is introduced [6, 20, 21]:

$$p_{GG}\left(\frac{P}{P_{R,sig}(1)}\right) = \frac{2(\alpha\beta)^{(\alpha+\beta)/2}}{\Gamma(\alpha)\Gamma(\beta)} A \left(\frac{P}{P_{R,sig}(1)}\right)^{\frac{\alpha+\beta}{2}-1} \times K_{\alpha-\beta}\left(2\sqrt{\alpha\beta\frac{P}{P_{R,sig}(1)}}\right). \tag{7}$$

From Eq. [6], the quantities were considered within the cases 1 and 2, additionally, the nominal range of optical power received goes for -30 dBm. Therefore, computations can be done pretending the value of A as constant is unity as in Eq. (7), furthermore the accurate estimate can be estimated to, in which refers to the value obtained in Case 2 assuming that refractive index structure in Case 1 minus such. We plotted the curve that represents Case 2 in Figure 3 and applied the same amount to. Given that Figure 5's values of Assuming that Cases 1 and 2 coincide with an average received optical power of -30 dBm, it can be established within the limits associated on integration combined with augmentation employed in the above Equations (2), (4), and (5) appropriate. The experiment's flaw, though, is that it ignores A's degree of divergence from 1. Of course, if one is trying to get curves that match reality, it can't go over a few percent.
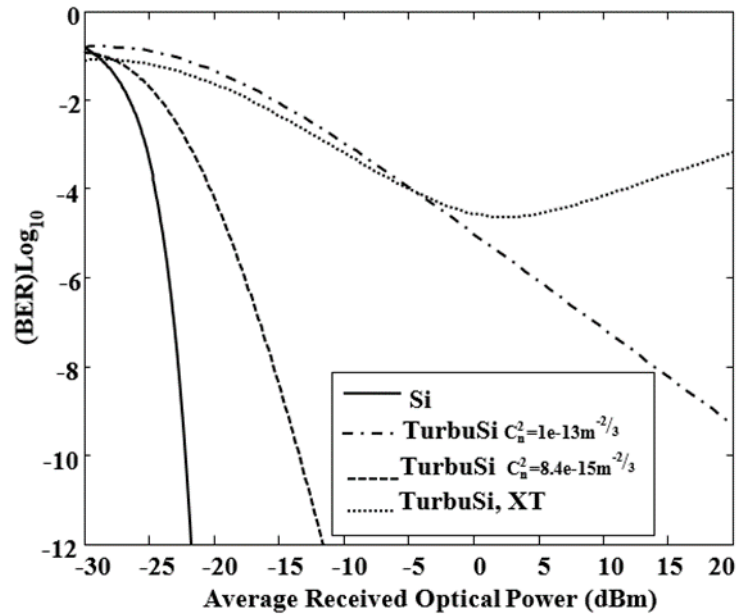
Figure 5. Log $_{10}$BER in comparison to the mean optical power of the received signal (dBm) in turbulence regimes C_{XT} = 30 dB.

6. Simulation Results

Analysis based on the outcomes in the simulation for system designed for DWDM-FSO investigation throughout noise with certain attributes that include interchannel crosswalk, and turbulence due to atmospheric instability emphasized is shown in this section [17–21]. Figure 6 illustrates free-space optical distribution of DWDM utilizing the lines codes of RZ and NRZ. To create the system enhancement, Opti system software is applied. The optimal multiplexer is then used to multiplex these channels. 100 GHz is the frequency spacing, and the starting frequency is 1550 nm. NRZ and RZ are the types of modulation. Attenuation and geometrical loss are the two primary factors that determine how much the laser output is attenuated. Equation 8 can be expressed from [17], [18], and [20]

$$P_{\text{Re}\,cieved} = P_{Transmitted}\,\frac{d\,r^2}{(d_t + \theta R)}\,10^{-\alpha\frac{R}{10}}$$
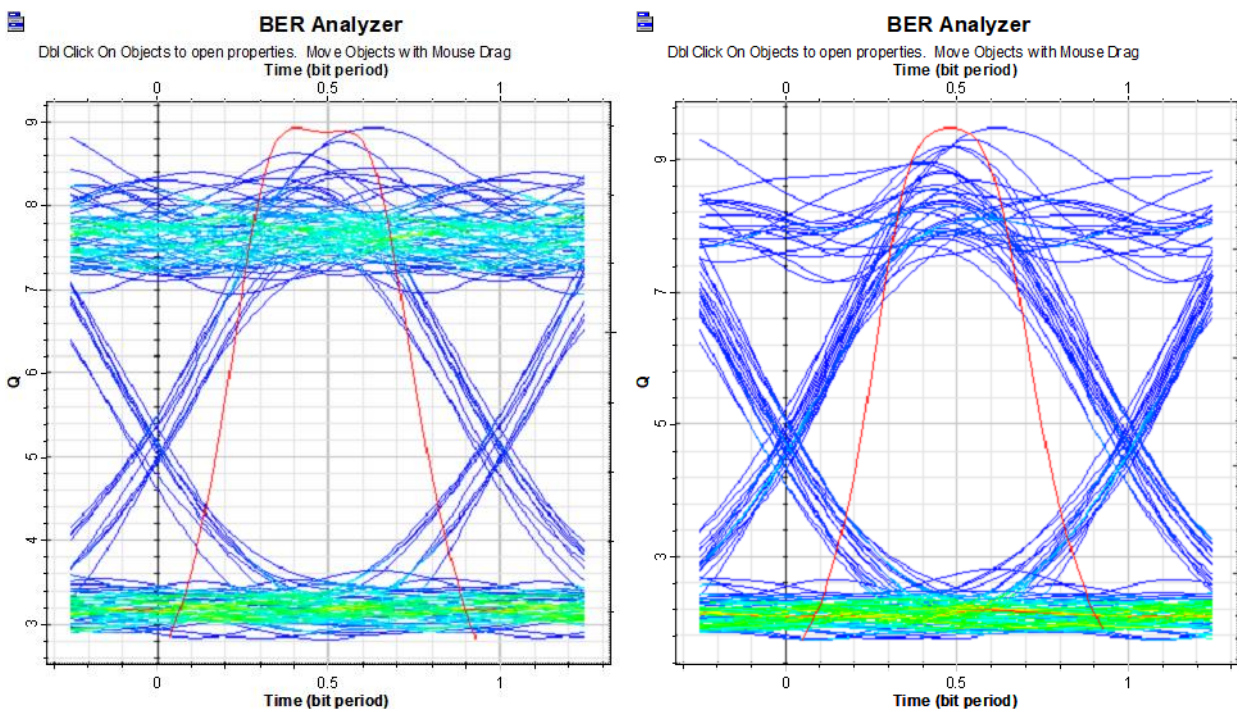
$$(8)$$

Figure 6. Simulated eye illustrations employing for 8-channel based DWDM-FSO under (a) NRZ line codes (b) RZ line

Table 1. BER and quality factor computations' outcomes

Methods of modulations	Quality factor	BER
NRZ	9.0132	2.0121e-019
RZ	9.5123	8.2134e-022

7. Conclusion

The article delves into the design and functionality of a DWDM-PON/FSO scheme with a focus on addressing the ever-growing bandwidth needs and traffic demands in modern networks. The analysis of the DWDM-FSO channel sheds light on critical factors such as noise, spatial interference issues, and interchannel crosstalk. Moreover, the article highlights the potential inaccuracies that can arise from the mathematical calculations involved, particularly when dealing with OOK modulation and the adaptive threshold. By exploring the intricacies of these technologies and their interplay, the article underscores the complexities inherent in optimizing data transmission efficiency while minimizing errors. The results suggest that careful consideration must be given to various variables and parameters to ensure reliable and robust network performance. In conclusion, the discussed DWDM-PON/FSO model represents a promising solution for enhancing network capabilities and meeting the escalating demands for higher bandwidth and data traffic. However, further research and refinement may be necessary to address the challenges associated with signal interference, error rates, and modulation techniques to fully realize the potential of this integrated scheme in modern telecommunications systems.

References

1. Chan, V. W. S. (2006). Free-space optical communications, *IEEE/OSA J. Lightw. Technol.*, 24(12), 4750_4762.
2. Shapiro, J. H.& Harney, R. C. (1980). Burst-mode atmospheric optical communication, *Proc. Nat. Telecommun. Conf.,* pp. 27.5.1_27.5.7.
3. J. Li, J. Q. Liu, and D. P. Taylor, `Optical communication using subcarrier PSK intensity modulation through atmospheric turbulence channels,'' IEEE Trans. Commun., vol. 55, no. 8, pp. 1598_1606, Aug. 2007.
4. Jurado-Navas, A., Garrido-Balsells, J. M., Castillo-Vazquez, M., Puerta-Notario, A. (2012). Closed-form expressions for the lower-bound performance of variable weight multiple pulse-position modulation optical links through turbulent atmospheric channels, *IET Commun.*, 6(4), 390–397.
5. Yang, L., Song, X., Cheng, J., Holzman J. F. (2016). Free-Space optical communications over lognormal fading channels using OOK with finite extinction ratios, *IEEE Access*, 4, 574-584.
6. Aladeloba, A. O., Woolfson, M. S., Phillips, A. J., (2013). WDM FSO network with turbulence-accentuated interchannel crosstalk, *IEEE/OSA.*, vol. 5(6), 641–651.
7. Ciaramella, E., Arimoto, Y., Contestabile, G., Presi, M., D'Errico, A., Guarino, V., Matsumoto, M., (2009). 1.28 terabit/s (32 × 40 Gbit/s)WDM transmission system for free space optical communications, *IEEE J. Sel. Areas. Commun.*, 27(9), 1639–1645.
8. Karp S. Gagliardi, R. M., Moran S. E., Stotts L. B., (1988). Optical Channels: Fibers, Clouds, Water and the Atmosphere. New York: *Plenum.*
9. Ramaswami R. & Sivarajan K. N., (2002). Optical Networks—*A Pratical Perspective, 2nd ed. London: Academic.*
10. Manor H. & Arnon S., (2003). Performance of an Optical Wireless Communication System as a Function of Wavelength, *Applied Optics*, 42(21), 4285-4294.
11. Arnon S. (2013). Optical Wireless Communications, *Encyclopedia of Optical Engineering*, 1866-1886.
12. Ansari N., Zhang J. (2013) Media access control and resource allocation for next generation passive optical networks, *Springer*.
13. Zuo T. J, Phillips A. J. (2009). Performance of burst mode receivers for optical digital pulse position Modulation in passive optical network application', *IET Optoelectron.*, 3, (3), 123-130.
14. Monroy I. T. & Tangdiongga E. (2002). Crosstalk in WDM Communication Networks. Norwell, MA: Kluwer Academic, 2002.
15. Andrews, L. C., Phillips, R. L. (2005). Laser beam propagation through random media' (SPIE Press, Bellingham, Washington, 2nd edn.).
16. Majumdar, A. K. (2005). Free-space laser communication performance in the atmospheric channel', *J. Opt. Fiber Commun. Rep.*, 2, 345–396.
17. Willebrand H. & Ghuman B. S. (2001). Fiber Optics without Fiber," IEEE, 2001.
18. Scott Bloom, (2002). Physics of free space optics,.

19. Elsayed E. E., Yousif B. B., Alzalabani M. M.(2018). Performance enhancement of the power penalty in DWDM FSO communication using DPPM and OOK modulation, *Opt. Quantum Electron.*, 50(7), doi: 10.1007/s11082-018-1508-y.

20. Elsayed E. E. & Yousif B. B., (2020). Performance enhancement of M-ary pulse-position modulation for a wavelength division multiplexing free-space optical systems impaired by interchannel crosstalk, pointing error, and ASE noise, *Opt. Commun.*, 475, doi: 10.1016/j.optcom.2020.126219.

21. Elsayed E. E. & Yousif B. B. (2020). Performance enhancement of the average spectral efficiency using an aperture averaging and spatial-coherence diversity based on the modified-PPM modulation for MISO FSO links," *Opt. Commun.*, 463, doi: 10.1016/j.optcom.2020.125463.

22. Elsayed, E. E. & Yousif , B. B. (2020). Performance evaluation and enhancement of the modified OOK based IM/DD techniques for hybrid fiber/FSO communication over WDM-PON systems, *Opt. Quantum Electron.*, 52(9), doi: 10.1007/s11082-020-02497-0.

23. Yousif, B. B., Elsayed, E. E., Alzalabani, M. M. (2019). Atmospheric turbulence mitigation using spatial mode multiplexing and modified pulse position modulation in hybrid RF/FSO orbital-angular-momentum multiplexed based on MIMO wireless communications system," *Opt. Commun.*, 436, 197–208. doi: 10.1016/j.optcom.2018.12.034.

24. Yousif, B. B. & Elsayed, E. E. (2019). Performance Enhancement of an Orbital-Angular-Momentum-Multiplexed Free-Space Optical Link under Atmospheric Turbulence Effects Using Spatial-Mode Multiplexing and Hybrid Diversity Based on Adaptive MIMO Equalization," *IEEE Access*, 7, 84401–84412. doi: 10.1109/ACCESS.2019.2924531.

25. Elsayed E. E. & Yousif, B. B. (2020). Performance enhancement of hybrid diversity for M-ary modified pulse-position modulation and spatial modulation of MIMO-FSO systems under the atmospheric turbulence effects with geometric spreading, *Opt. Quantum Electron.*, 52(12). doi: 10.1007/s11082-020-02612-1.